THE JOURNAL OF BIOLOGICAL CHEMISTRY VOL. 288, NO. 1, pp. 520–528, January 4, 2013

Murine Hyaluronidase 2 Deficiency Results in Extracellular Hyaluronan Accumulation and Severe Cardiopulmonary Dysfunction*

Received for publication, June 20, 2012, and in revised form, November 19, 2012 Published, JBC Papers in Press, November 21, 2012, DOI 10.1074/jbc.M112.393629

Biswajit Chowdhury[‡1], **Richard Hemming**[‡], **Sabine Hombach-Klonisch**[§¶‖], **Bruno Flamion**[**], **and Barbara Triggs-Raine**[‡‖2]

From the [‡]*Departments of Biochemistry and Medical Genetics,* [§]*Human Anatomy and Cell Science,* [¶]*Obstetrics, Gynecology and Reproductive Medicine, and* [‖]*Pediatrics and Child Health, Faculty of Medicine, University of Manitoba, Winnipeg, Manitoba R3E 0J9, Canada and the* [**]*Molecular Physiology Research Unit (URPHYM), Namur Research Institute for Life Sciences (NARILIS), University of Namur, B-5000 Namur, Belgium*

Background: The role of hyaluronidase 2 in hyaluronan degradation and cardiopulmonary function is largely uncharacterized.
Results: Hyaluronidase 2-deficient mice accumulate extracellular hyaluronan, leading to defective cardiopulmonary function.
Conclusion: Hyaluronidase 2 is essential for hyaluronan degradation and normal heart and lung health.
Significance: Our studies suggest that hyaluronidase 2 deficiency should be considered as a contributor to cardiac pathologies in humans.

Hyaluronidase (HYAL) 2 is a membrane-anchored protein that is proposed to hydrolyze hyaluronan (HA) to smaller fragments that are internalized for breakdown. Initial studies of a *Hyal2* knock-out (KO) mouse revealed a mild phenotype with high serum HA, supporting a role for HYAL2 in HA breakdown. We now describe a severe cardiac phenotype, deemed acute, in 54% of *Hyal2* KO mice on an outbred background; *Hyal2* KO mice without the severe cardiac phenotype were designated non-acute. Histological studies of the heart revealed that the valves of all *Hyal2* KO mice were expanded and the extracellular matrix was disorganized. HA was detected throughout the expanded valves, and electron microscopy confirmed that the accumulating material, presumed to be HA, was extracellular. Both acute and non-acute *Hyal2* KO mice also exhibited increased HA in the interstitial extracellular matrix of atrial cardiomyocytes compared with control mice. Consistent with the changes in heart structure, upper ventricular cardiomyocytes in acute *Hyal2* KO mice demonstrated significant hypertrophy compared with non-acute KO and control mice. When the lungs were examined, evidence of severe fibrosis was detected in acute *Hyal2* KO mice but not in non-acute *Hyal2* KO or control mice. Total serum and heart HA levels, as well as size, were increased in acute and non-acute *Hyal2* KO mice compared with control mice. These findings indicate that HYAL2 is essential for the breakdown of extracellular HA. In its absence, extracellular HA accumulates and, in some cases, can lead to cardiopulmonary dysfunction. Alterations in HYAL2 function should be considered as a potential contributor to cardiac pathologies in humans.

Hyaluronidase 2 is a glycophosphatidylinositol-linked protein and a member of the hyaluronoglucosaminidase family (1, 2). It is proposed to initiate the degradation of hyaluronan (HA),[3] an abundant glycosaminoglycan (GAG) in the extracellular matrix (ECM) of many vertebrate tissues (including heart valves), vitreous of the eye, and synovial fluid. The viscoelastic properties of HA influence the properties of the ECM and are important for cell proliferation, differentiation, and migration. A role for HA in embryogenesis has been established using HA synthase 2-deficient mice, which die at embryonic day 9.5 due to loss of endocardial cushion swelling and a lack of epithelial-to-mesenchymal transition (3).

Regulation of HA levels is required for normal development and to maintain normal tissue homeostasis. Degradation of HA by hyaluronidases (HYALs) is important for maintaining these levels. Six HYAL-encoding genes have been identified, which are grouped into two tightly linked triplets, one on human chromosome 3p21.3 (*HYAL1*, *HYAL2*, and *HYAL3*) and one on human chromosome 7q31.3 (*HYALP1*, *HYAL4*, and *SPAM1*) (4). With the exception of HYAL4 and HYALP1, all of the HYALs are thought to be capable of degrading HA. A role for HYAL1 and HYAL2 in HA degradation in somatic cells has been proposed. In this model, HYAL2 initiates HA degradation into small fragments that are endocytosed and degraded in lysosomes by HYAL1 and exoglycosidases (5, 6). HYAL2 is a glycosylphosphatidylinositol-anchored protein (2) that could act at low pH at the cell surface (7). It has been suggested that HYAL2 resides in lysosomes in some cell types (8). Despite the proposed role for HYAL2 in HA degradation, only a deficiency of HYAL1 has been found to cause a human disorder. It causes mucopolysaccharidosis (MPS) IX, a lysosomal storage disorder

* This work was supported in part by Canadian Institutes of Health Research Grant MP-89873.
[1] Supported by a joint studentship from the Manitoba Health Research Council and the University of Manitoba.
[2] To whom correspondence should be addressed: Dept. of Biochemistry and Medical Genetics, 745 Bannatyne Ave., University of Manitoba, Winnipeg, Manitoba R3E 0J9, Canada. Tel.: 204-789-3218; Fax: 204-789-3900; E-mail: traine@cc.umanitoba.ca.

[3] The abbreviations used are: HA, hyaluronan; GAG, glycosaminoglycan; ECM, extracellular matrix; HYAL, hyaluronidase; MPS, mucopolysaccharidosis; KO, knock-out; HABP, HA-binding protein; α-SMA, α-smooth muscle actin.

characterized by joint abnormalities due to HA accumulation (9, 10).

In the heart valves, GAGs are abundant and play important roles in both developing and mature valves (11, 12). It is not surprising that cardiovascular manifestations are a prominent feature of many forms of MPS that result from GAG accumulation (13). For example, mitral valve thickening and stenosis are found in Hurler and Scheie diseases, and these findings are also reflected in the corresponding mouse model (14). Therefore, defects in ECM-modifying enzymes are among the many causes of cardiovascular disease.

HA is one of the major GAGs in heart valves. Surprisingly, no broad-spectrum HA accumulation, including in the heart, was identified during the characterization of *Hyal1*-, *Hyal2*-, or *Hyal3*-deficient mice (15–17). Previous studies of *Hyal2*$^{-/-}$ (knock-out (KO)) mice revealed craniofacial abnormalities and chronic anemia, as well as unexplained preweaning lethality (16). However, in addition to these features, on an outbred background (C129;CD1;C57BL/6), we have found a gross enlargement of either the left or right atrium in more than half of the *Hyal2* KO mice that survived to weaning. Because HA synthesis is known to be essential for normal heart development, we hypothesized that a failure to degrade HA in these mice had resulted in HA accumulation, leading to cardiopulmonary dysfunction and premature death.

EXPERIMENTAL PROCEDURES

Generation of Hyal2 KO Mice—Hyal2 KO mice were generated as part of a previous study (16). For this study, *Hyal2* KO mice and control littermates, either wild type (+/+) or heterozygous (+/−), on an outbred background (C129;CD1;C57BL/6) were derived through breeding of *Hyal2* heterozygotes. Mice were genotyped using PCR-based strategies on DNA samples isolated from ear punches. For amplification of wild type *Hyal2* and the Neo-targeted *Hyal2* allele, we used forward and reverse primers (5′-actcagctgctggttcccta-3′ and 5′-atagcactggcagcgaaagt-3′; 5′-aaggaacatcagggaagatcat-3′ and 5′-cggtgcccgagactaagtc-3′, respectively). All animal procedures were conducted following protocols approved by the University of Manitoba Animal Care Committee and following the guidelines of the Canadian Council on Animal Care.

Histology—Mice were killed by carbon dioxide inhalation, and tissues for light microscopy were immediately collected and fixed overnight in either formalin or 10% buffered formalin (PROTOCOL) containing 1% hexadecylpyridinium chloride monohydrate. Tissues for subsequent biochemical studies were stored at −80 °C. Fixed tissues were embedded in paraffin, and 5-μm sections were stained for morphological analysis using established methods for hematoxylin and eosin (18) or for GAG detection using Alcian blue (19), with minor modifications in the time of incubation with the stain. Counterstaining for Alcian blue was performed with Nuclear Fast Red (ScyTek Laboratories) for 2.5 min. Heart and lung ECM was stained using Masson's trichrome stain (Sigma-Aldrich) according to the manufacturer's protocol. Slides were dehydrated, mounted, and visualized using bright-field microscopy. For analysis of hypertrophy in cardiomyocytes, slides were incubated for 30 min with 4 μg/ml wheat germ agglutinin (Alexa Fluor® 488 conjugate), mounted using Prolong Gold (Invitrogen), and visualized by fluorescence microscopy. The area of the cardiomyocytes, as defined by binding to wheat germ agglutinin, was measured using AxioVision 4.5 software. A minimum of seven fields, containing an average of eight cells per field, was examined for each animal.

Electron Microscopy—The valve and surrounding myocardium were collected by punch biopsy from a whole heart that was sliced using a rodent heart slicer matrix (Zivic Instruments). Tissues were fixed for 4 h at room temperature in 2% glutaraldehyde and 2% paraformaldehyde prepared in 100 mM sodium cacodylate buffer (pH 7.2) containing 10 mM $CaCl_2$ and 0.7% Ruthenium red. After fixation, tissues were washed with buffer containing 100 mM sodium cacodylate, 10 mM $CaCl_2$, 0.7% Ruthenium red, and 0.7% sucrose (pH 7.2) for 5 min, 30 min, and 1 h at room temperature. Tissues were post-fixed for 1 h in 100 mM sodium cacodylate containing 1% osmium tetroxide and 0.7% Ruthenium red, followed by three 10-min washes with double-distilled H_2O. Tissues were dehydrated for 10 min each in 50% ethanol, 75% ethanol, 95% ethanol, two changes in 100% ethanol followed by 100% methanol, and three changes in propylene oxide. After dehydration, tissues were infiltrated by incubation in a mixture of propylene oxide and Araldite 502 (58.9:46:2% (w/v) mixture of Araldite, dodecenyl succinic anhydride, and 2,4,6-Tris (dimethylaminomethyl) phenol-30; Ted Pella, Inc.). The infiltration solutions were prepared with propylene oxide and Araldite (3:1, 1:1, and 1:3) and incubated for 1 h each. Slow hardening of the Araldite was performed through 1-day incubations at room temperature, 45 °C, and 60 °C.

Detection of HA, α-Smooth Muscle Actin, F4/80, and CD31—HA was detected with biotinylated HA-binding protein (HABP; Calbiochem) as described previously (17), except without enzyme retrieval and using HABP (1.67 μg/ml for heart and 6.68 μg/ml for lungs) in Tris-buffered saline (pH 7.5) overnight at 4 °C. Sections were incubated with avidin-conjugated horseradish peroxidase, detected with diaminobenzidine, and counterstained with Nuclear Fast Red. To verify the specificity of HABP, sections were incubated overnight with 25 units/ml HYAL from *Streptomyces hyalurolyticus* (Sigma) before HABP detection.

For detection of α-smooth muscle actin (α-SMA), F4/80, and CD31, the sections were incubated overnight at 4 °C with mouse monoclonal anti-human smooth muscle actin (1:300; Dako), rat monoclonal anti-mouse F4/80 (1:100; AbD Serotec), or rabbit polyclonal anti-CD31 (1:50; Abcam) antibody, respectively. Secondary antibodies (biotinylated rabbit anti-mouse (1:1000; Dako) or goat anti-rat (1:500; Invitrogen)) were used to detect the primary complexes, and complex detection was as described above for HA. For F4/80 and CD31, antigen retrieval was performed by incubating the slides for 20 min at 95 °C in 10 mM sodium citrate (pH 6).

Analysis of HA Concentration and Sizes—Blood was collected from mice immediately following euthanasia or from the saphenous vein of living mice at 6 and 12 weeks. Serum was collected from clotted blood by centrifugation at 3000 rpm for 10 min and stored at −80 °C. HA levels were quantified using an ELISA-like HA test plate (R&D Systems) according to the man-

ufacturer's directions. All samples were analyzed in duplicate, and the average value was used for subsequent comparisons.

Fluorophore-assisted carbohydrate electrophoresis was performed for quantification of HA and chondroitin sulfate in tissues (20). Briefly, GAGs isolated from frozen heart tissue by 50 μg/μl proteinase K digestion and ethanol precipitation were cleaved to disaccharide units by overnight incubation with hyaluronidase SD (Seikagaku catalog no. 100741-1) or chondroitinase ABC (Sigma-Aldrich) in 200 mM ammonium acetate. The disaccharides were isolated, labeled with 2-aminoacridone, and quantified in comparison with known disaccharide standards as described previously (21). Fluorescence was detected using the Fluor-S Max MultiImager (Bio-Rad) and quantified using Quantity One 4.6.9 software (Bio-Rad).

For sizing of HA, GAGs were prepared from tissue (10–15 mg) or serum (200–400 μl) as for fluorophore-assisted carbohydrate electrophoresis, except 5 mM deferoxamine was included in the proteinase K digestion, and a 4-h incubation at 37 °C with 10 units of DNase I and 50 μg of RNase A was incorporated after destroying the proteinase K by boiling. Instead of digesting the GAGs to disaccharides, they were enriched by precipitation with 1% hexadecylpyridinium chloride monohydrate as described previously (22). The pellet was then resuspended in 100 μl of 20 mM Tris (pH 8.0), and Pronase was added to 0.2 mg/ml. Following overnight incubation, the GAGs were precipitated with 900 μl of 100% ethanol. The final pellet was resuspended in 15 μl of water, 3 μl of Orange G tracking dye was added, and the sample was separated by electrophoresis on a 0.8% agarose gel prepared in Tris acetate buffer (pH 8.3). The gel was stained overnight with 0.005% Stains-all prepared in 50% ethanol, destained with 10% ethanol until the bands were clearly visible, and photographed. Negative control samples to verify the identity of the HA were prepared by incubating the GAGs overnight with 2.5 units of hyaluronidase SD before they were analyzed by electrophoresis.

Statistical Analysis—The genotype distributions were compared with the expected Mendelian ratios using the χ^2 test. For all other statistical analysis, data are presented as means ± S.E. Means were compared by Student's *t* test. $p \leq 0.05$ was considered statistically significant.

RESULTS

Increased Mortality in Hyal2 KO Mice—We obtained viable *Hyal2* KO mice by intercrossing *Hyal2* heterozygotes (+/−); although as reported previously (16), preweaning lethality was observed. In fact, only ~9% (70 of 789) of the offspring were *Hyal2* KOs at weaning instead of the expected Mendelian 25% ($\chi^2_2 = 109.86$; $p < 0.001$). Of the viable *Hyal2* KO mice, 54% were smaller in size than their littermates and exhibited rapid onset lethargy, weight loss, dull coat, and shortness of breath requiring euthanasia at an average of 3.2 months of age. Upon dissection, the left or right atrium of these mice was grossly dilated (Fig. 1). The remaining 46% of *Hyal2* KO mice developed a slower onset lethargy, loss of weight, and poor grooming that required euthanasia at an average of 5.8 months of age. Severe atrial dilation was not found in these mice or in control littermates ($Hyal2^{+/+}$/$Hyal2^{+/-}$). However, one kidney was found to be missing in 1% of control mice and 43% ($n = 29$) of

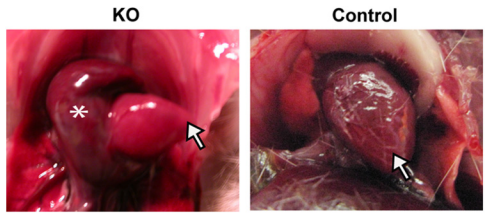

FIGURE 1. **Atrial dilation in *Hyal2* KO mice.** For orientation, the *arrows* indicate the apex of the *Hyal2* KO and control (+/+) hearts; the *asterisk* indicates the dilated atrium of the KO heart.

Hyal2 KO mice, suggesting that this phenotype is increased by *Hyal2* deficiency. The kidney phenotype was not further investigated, as it was found to be independent of the atrial dilation. For the studies described herein, the *Hyal2* KO mice were divided into two categories: mice with atrial dilation were defined as "acute," and those without atrial dilation were defined as "non-acute."

Heart Valve Expansion in Hyal2 KO Mice—The atrial dilation in the acute *Hyal2* KO mice, together with the knowledge that HA is abundant in the heart valve, led us to look for a valve abnormality in the *Hyal2* KO mice. H&E staining revealed a profound expansion of the pulmonary, mitral, aortic, and tricuspid valves in all mice that were examined ($n = 9$) compared with control littermates ($n = 7$). Representative sections of the pulmonary and mitral valves are shown in Fig. 2 (*A*–*D*). To determine whether there was any difference in the expansion of the valves in the acute and non-acute *Hyal2* KO mice, we compared the expansion/length of the valve leaflet/cups by determining the number of serial sections that included each valve. The valve thickness was significantly greater in *Hyal2* KO mice than in control mice, but there was no significant difference between acute and non-acute *Hyal2* KO mice (Fig. 2*E*).

Structure/Organization of Valves in Hyal2 KO Mice—To determine whether HA was accumulating in the *Hyal2* KO mice, we used HABP to detect HA. Abundant HA was found throughout the valves (Fig. 3, *A*–*J*), and given the expanded size of the valves in the *Hyal2* KO mice, this indicates that HA was accumulating in the *Hyal2* KO valves.

To determine whether the accumulating HA was altering the organization of the ECM of the valve, we examined ECM components using Masson's trichrome stain. Compared with normal valves (Fig. 4*B*), those from *Hyal2* KO mice were disorganized, with GAGs (white material) deposited between the collagen fibers in the fibrosa and ventricularis/atrialis layers, respectively, and resulting in an expanded spongiosa layer (Fig. 4*A*). Endothelial cells in the valve were identified by staining for the endothelial marker CD31. The CD31-positive cells (brown) appeared less frequently in the *Hyal2* KO valve, probably because these cells were stretched over the extended surface area of the expanded valve (Fig. 4, *C* and *D*). These findings indicate that the accumulated HA in the ECM of *Hyal2* KO mice leads to the expansion, thickening, and disorganization of the valve leaflet/cups.

We also examined the structure of the atrial and ventricular myocardium of acute and non-acute *Hyal2* KO mice and control mice for additional pathologies. Staining for total GAG with Alcian blue revealed accumulation of interstitial GAGs

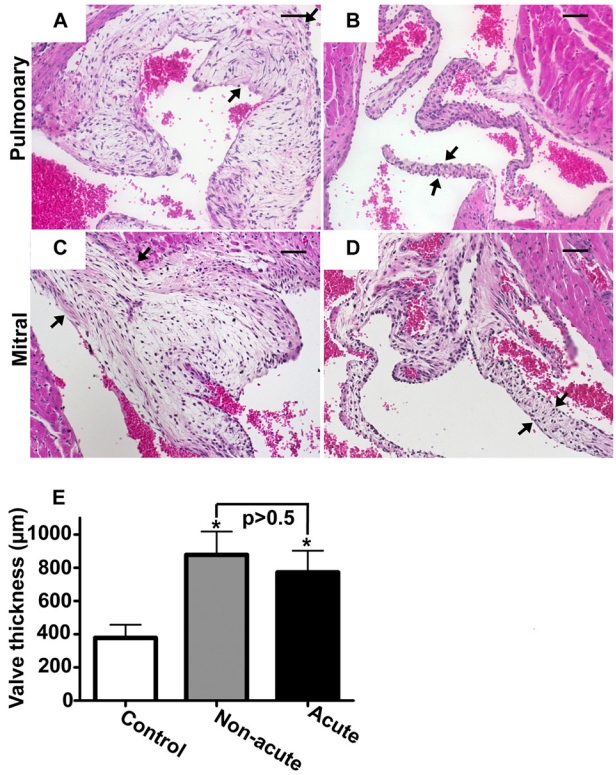

FIGURE 2. **Histopathology of heart valves.** *A–D*, H&E stains of cross-sections of the hearts of *Hyal2* KO (*A* and *C*) and control (*B* and *D*) mice. Representative photographs of the pulmonary (*A* and *B*) and mitral (*C* and *D*) valves show the expansion in the *Hyal2* KO mice (*arrows* indicate valve edges). *E*, comparison of the valve thickness in *Hyal2* KO and control (+/− and +/+) mice. Thickness was estimated by determining the total number of 5-μm serial cross-sections that included any of the four heart valves. Graphed values represent the mean thickness ± S.E. Significant expansion of the valves in *Hyal2* KO mice compared with control littermates ($n = 4$; *, $p < 0.05$) was found, but there was no significant difference between non-acute and acute *Hyal2* KO mice ($n = 4$; $p = 0.60$). *Scale bars* = 50 μm.

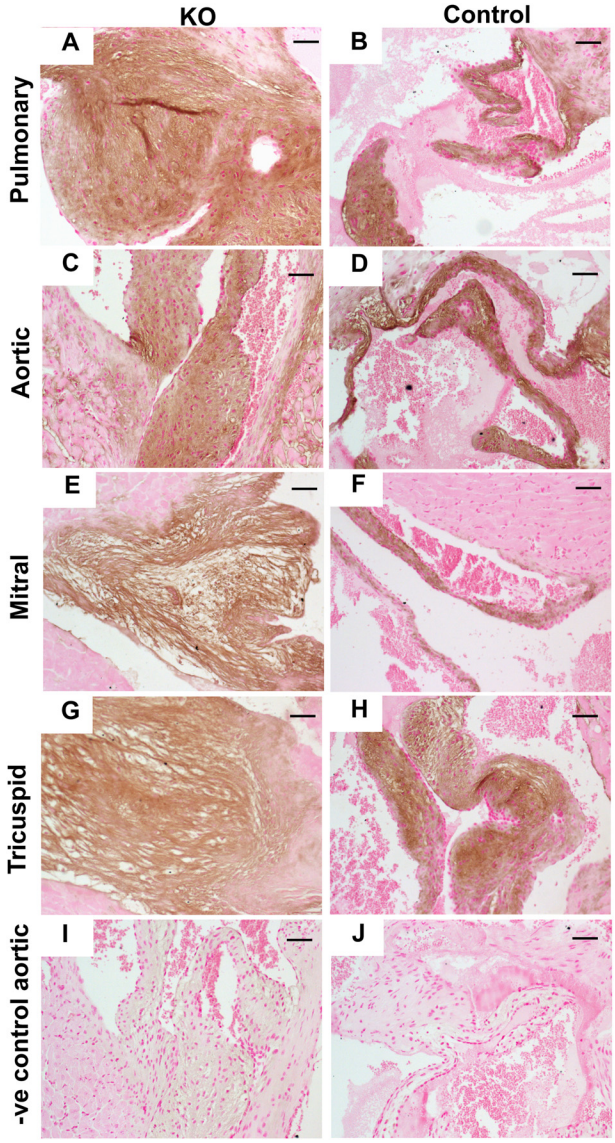

FIGURE 3. **Analysis of HA in heart tissues.** *A–J*, detection of HA in cross-sections of the heart was performed using HABP. Representative results for all four valves are shown. The intensity of HA staining (*brown*) was similar throughout the *Hyal2* KO and control (+/−) valves. *I* and *J*, representative negative (−*ve*) controls for HABP staining. *Scale bars* = 50 μm.

between the atrial cardiac myocytes (Fig. 5, *A*, *C*, and *E*). This staining was more prominent in the acute *Hyal2* KO mice than in the non-acute *Hyal2* KO mice and was always stronger in *Hyal2* KO mice than in control mice, indicating that GAGs were accumulating in the KO mice. In adjacent serial sections, HA was found to be abundant in the ECM of the acute mice compared with both the non-acute and control mice (Fig. 5, *B*, *D*, and *F*), providing further evidence that HA was accumulating in the *Hyal2* KO mice.

Cardiac Hypertrophy in Hyal2 KO Mice—To determine whether there were additional abnormalities in the cardiac myocytes of *Hyal2* KO mice, sections were stained with fluorescently labeled wheat germ agglutinin, and the sizes of the cardiomyocytes were determined. Significant cardiac hypertrophy was found in the upper ventricular region, close to the base of the heart, of acute *Hyal2* KO mice compared with control mice (Fig. 6*A*), but this hypertrophy did not reach significance in the lower ventricular region of acute *Hyal2* KO mice (Fig. 6*B*) or non-acute *Hyal2* KO mice (Fig. 6, *C* and *D*).

Accumulation of ECM in Hyal2 KO Hearts—To further characterize the changes in the *Hyal2* KO hearts, we performed transmission electron microscopy on the valves and the ventricular and atrial myocardium. In the control valves (Fig. 7*E*), the ECM was densely packed with collagen fibrils, whereas in the *Hyal2* KO valves (Fig. 7*A*), the ECM separated the collagen fibrils. The accumulated material in the *Hyal2* KO valves was clearly extracellular and was presumed to be HA. The atrial myocardium of *Hyal2* KO mice (Fig. 7, *B* and *C*) contained cardiomyocytes, which showed a disorganized arrangement of myofibrils and mitochondria and a substantial reduction in myofibrils. In contrast, the atrial cardiomyocytes of control mice showed a sarcoplasm with tightly packed myofibrils and mitochondria (Fig. 7, *F* and *G*). Within the ventricular myocardium, we observed cardiomyocytes with a disorganized arrangement of myofibrils and mitochondria and a more loosely packed sarcoplasm (Fig. 7*D*) compared with controls (Fig. 7*H*).

Histopathology of Lungs of Hyal2 KO Mice—To look for additional differences in acute, non-acute, and control mice that might be related to atrial dilation, we examined the lungs. A

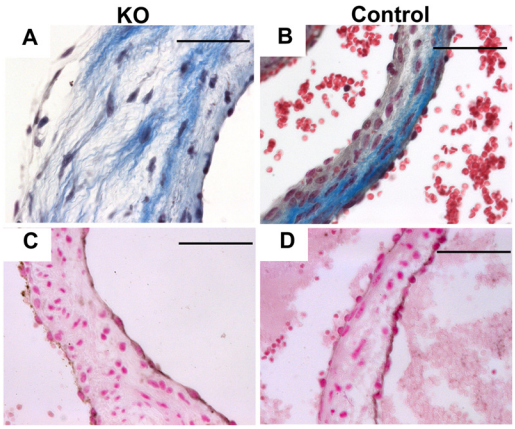

FIGURE 4. **Analysis of valvular organization.** *A* and *B*, Masson's trichrome staining of aortic valves showed increased GAGs (white) separating the collagen fibers (*light blue*) in *Hyal2* KO mice (*A*) compared with control mice (+/−) (*B*). *C* and *D*, anti-CD31 antibodies were used to detect endothelial cells (*brown*) on the valve surface in *Hyal2* KO and control (+/+) mice. CD31-positive cells were found to be closely spaced on the control valves (*D*) but widely spaced on the *Hyal2* KO valves (*C*). *Scale bars* = 50 μm.

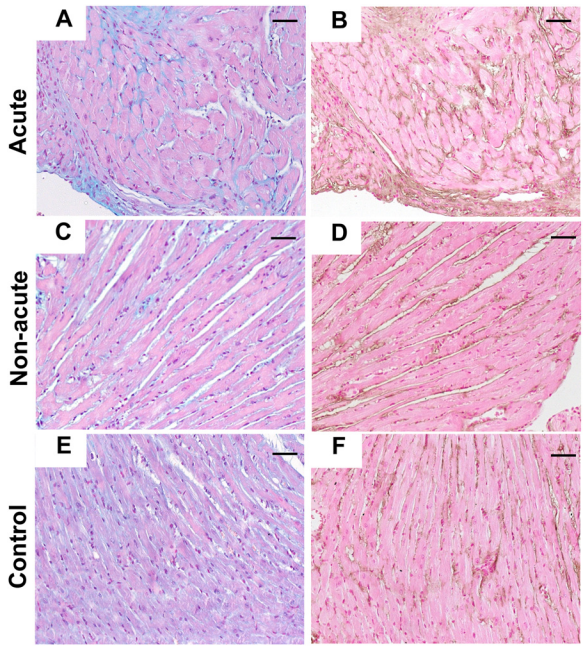

FIGURE 5. **Analysis of GAGs in the myocardium.** Representative examples of Alcian blue-stained myocardium show increased intercellular GAG accumulation in the acute *Hyal2* KO mice (*A*) compared with the non-acute *Hyal2* KO (*C*) and control (*E*) mice. Enhanced HABP staining (*brown*) of consecutive serial slides showed the presence of more HA in the acute mice (*B*) than in the non-acute (*D*) and control (*F*) mice. *Scale bars* = 50 μm. The genotype of the control animals is +/+.

dramatic difference between the acute and non-acute *Hyal2* KO lungs was identified. The alveoli were reduced, and the alveolar septa were thickened in the acute *Hyal2* KO mice compared with the non-acute and control mice (Fig. 8, *A–C*). Further, Masson's trichrome staining revealed increased collagen in the alveolar septa of the acute mice that was absent in both the non-acute and control mice (Fig. 8, *D–F*). Further investigation of the thickened alveolar septa using anti-α-SMA immunostaining revealed a strong signal for α-SMA in the alveolar interstitium of acute mice that was not detected in the lungs of non-acute and control mice (Fig. 8, *G–I*). Increased levels of HA

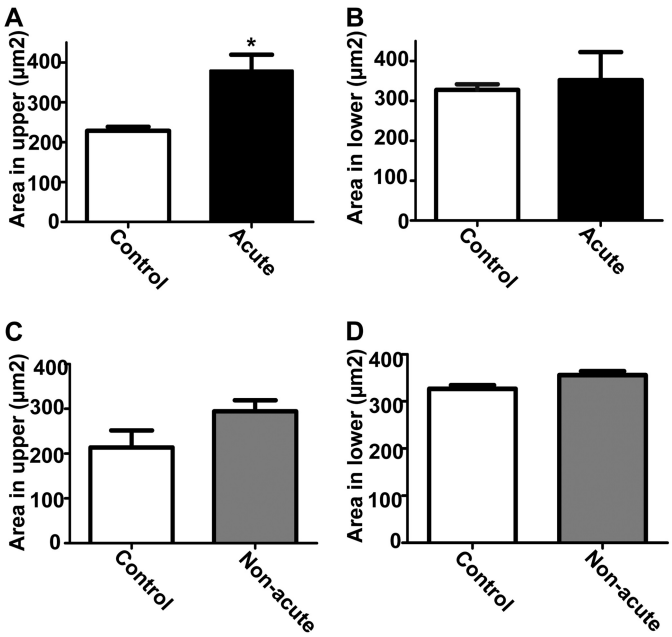

FIGURE 6. **Cardiac hypertrophy in *Hyal2* KO mice.** *A*, cardiomyocytes of the upper ventricular myocardium showed significant hypertrophy in acute *Hyal2* KO mice compared with control mice ($n = 3$; *, $p < 0.05$). *B*, the lower ventricular myocardium showed no significant difference between acute *Hyal2* KO and control mice ($n = 3$; $p = 0.74$). Graphed values are expressed as means ± S.E. The size of the cardiomyocytes of the upper (*C*) and lower (*D*) ventricular myocardium of non-acute *Hyal2* KO and control mice ($n = 3$; $p = 0.14$ and 0.06) did not differ significantly. Graphed values represent means ± S.E. The control data presented are from mice with both +/+ and +/− genotypes.

were also detected in the lungs of acute and non-acute *Hyal2* KO mice compared with control mice (Fig. 8, *J–L*), although the levels were much higher in the acutely affected animals. Therefore, pathology typical of severe pulmonary fibrosis was present only in the acute *Hyal2* KO mice. We observed numerous alveolar macrophages (foam cells) in the inter- and intra-alveolar spaces of acute and, to a lesser extent, non-acute *Hyal2* KO mice (Fig. 8, *A* and *B*) compared with control mice, suggesting that the accumulation of HA led to the recruitment of macrophages to the lung parenchyma. To confirm that these infiltrating cells were macrophages, we used an antibody against F4/80 (Fig. 8, *M–O*).

Increased HA Levels and Size in Hyal2 KO Sera and Hearts—A deficiency of HYAL2 had already been demonstrated to lead to increased serum HA (16). As expected, we found the levels of HA to be ~19-fold higher in *Hyal2* KO mice compared with control mice at 12 weeks (Fig. 9*A*). The levels of HA increased with age in the *Hyal2* KO mice, reaching an average 27-fold increase at the time of euthanasia (Fig. 9*A*). Interestingly, the levels of serum HA were elevated in both acute and non-acute *Hyal2* KO animals, indicating that differences in the levels of circulating HA are unlikely to be the cause of the more severe phenotype in acute *Hyal2* KO animals.

We also quantified the levels of HA in the hearts and lungs of *Hyal2* KO mice using fluorophore-assisted carbohydrate electrophoresis. Consistent with the detection of increased HA by immunohistochemistry, elevated levels of HA were found in *Hyal2* KO hearts and lungs compared with control mice (Fig. 9, *B* and *C*). No significant difference between the levels of HA in

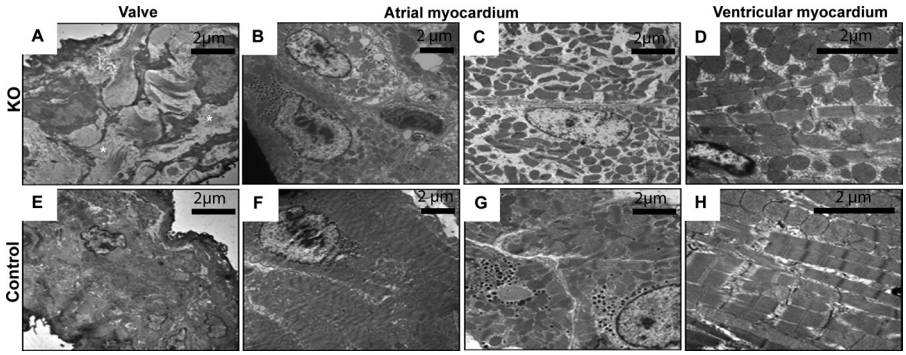

FIGURE 7. **Subcellular structure of *Hyal2* KO heart tissues.** Representative transmission electron microscopy images are shown for *Hyal2* KO (*A–D*) and control (*E–*) mice. Compared with the organization of the ECM in the valves of control mice (*E*), the extracellular space in the *Hyal2* KO mouse valve (*A*) contained excessive GAG accumulation (*, *white space*) between the fibroblasts, causing separation of the collagen fibrils. The atrial myocardium in *Hyal2* KO mice contained cardiomyocytes lacking an organized arrangement of myofibrils and mitochondria (*B*) and showing reduced myofibrils (*C*). In contrast, the atrial cardiomyocytes of control mice showed tightly packed myofibrils and mitochondria (*F* and *G*). We observed a disorganized arrangement of myofibrils and mitochondria within a more loosely packed sarcoplasm in ventricular cardiomyocytes of *Hyal2* KO mice (*D*) compared with control mice (*H*). All control mice (*E–H*) for this study were +/−.

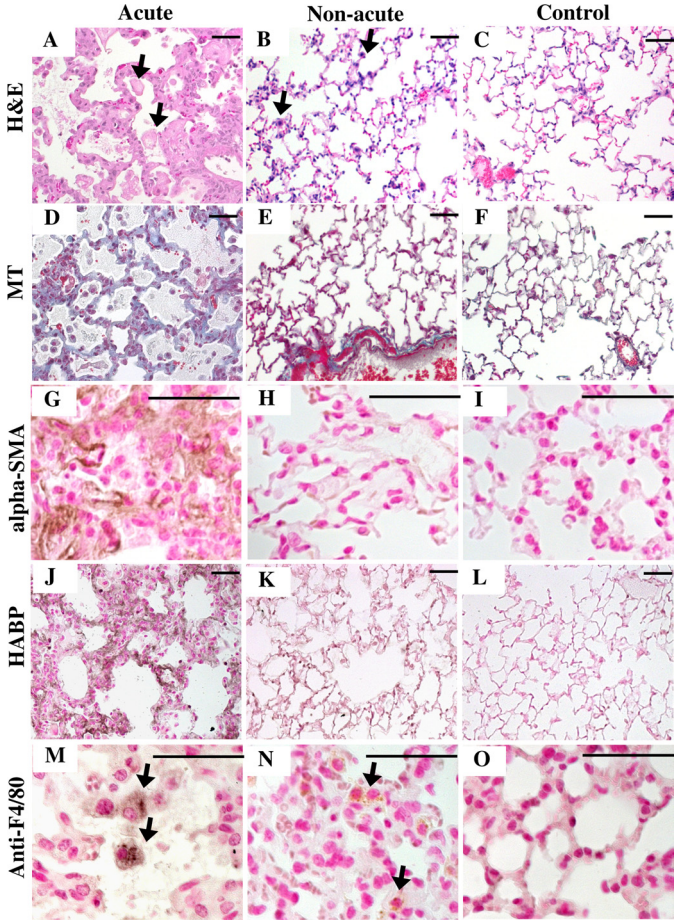

FIGURE 8. **Histopathology of lungs.** *A–C*, H&E staining of alveolar structure in acute (*A*), non-acute (*B*), and control (*C*) mice. Acute mice showed dilated alveoli and thickened septa compared with the other two groups. *D–F*, Masson's trichrome (*MT*) staining showed the accumulation of collagen (*light blue*) in acute mice (*D*) compared with non-acute (*E*) and control (*F*) mice. *G–I*, staining for α-SMA (*brown*) clearly showed the presence of α-SMA in the alveolar septa of acute mice (*G*) but not non-acute (*H*) or control (*I*) mice. *J–L*, staining for HABP (*dark brown*) clearly showed the presence of more HA in the alveolar septa of acute mice (*J*) compared with non-acute (*K*) and control (*L*) mice. Alveolar macrophages (foam cells; *arrows*) were found in acute (*M*) and non-acute (*N*) mice compared with control mice (*O*). *Scale bars* = 50 μm. Genotypes of control mice were +/+ in *C*, *F*, and *L* and +/− in *I* and *O*.

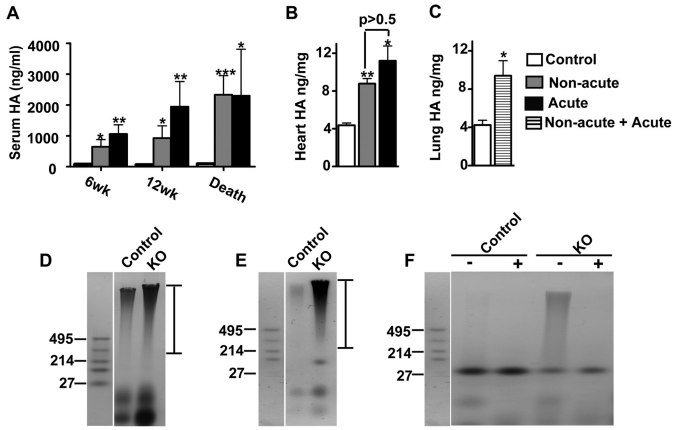

FIGURE 9. **Serum and tissue HA content and size in *Hyal2* KO mice.** *A*, mean serum HA levels in control mice and non-acute and acute *Hyal2* KO mice at 6 weeks (*wk*; control, $n = 7$; non-acute, $n = 5$; and acute, $n = 4$), 12 weeks (control, $n = 6$; non-acute, $n = 5$; and acute, $n = 3$), and at death (control, $n = 15$; non-acute, $n = 11$; and acute, $n = 7$). The levels of HA in the serum were significantly increased in non-acute and acute *Hyal2* KO mice compared with control mice. *B*, total HA content in the heart ($n = 3$ in each group). The amount of HA was significantly increased in non-acute and acute *Hyal2* KO mice compared with control mice, but acute and non-acute mice did not differ from one another ($p = 0.22$). *C*, total HA content in the lung ($n = 3$ in each group). The amount of HA was significantly increased in the lungs of *Hyal2* KO mice compared with control mice ($p = 0.04$). Graph values are expressed as means ± S.E. *, $p < 0.05$; **, $p < 0.001$; ***, $p < 0.0001$ (Student's *t* test). The control data presented were from both +/+ and +/− mice. HA size in the hearts (*D*) and sera (*E*) of *Hyal2* KO and control mice was analyzed by agarose gel electrophoresis of GAGs isolated from these tissues. The sizes of HA standards (Select-HA LoLadder, Hyalose) in kilodaltons are shown to the left of *D–F*. The dark-staining high molecular mass material, spanning the region indicated by the *bars* to the right of *D* and *E*, is HA. *F*, to differentiate HA within the stained material on the agarose gel from other GAGs and contaminating proteins, GAGs isolated from the sera of control and *Hyal2* KO mice were not treated (−) or treated (+) with HYAL and then analyzed by agarose gel electrophoresis. The high molecular mass material was removed by HYAL treatment, identifying it as HA.

non-acute and acute *Hyal2* KO mice was detected in the heart (Fig. 7*B*). The HA levels also appeared similar in the lungs of acute and non-acute *Hyal2* KO mice, but our sample size was not large enough for statistical analysis. We also examined the chondroitin sulfate levels in the heart by fluorophore-assisted carbohydrate electrophoresis, and no significant difference

between *Hyal2* KO (0.91 ± 0.17 ng/mg) and control (0.77 ± 0.12 ng/mg) mice was found ($n = 4$; $p = 0.51$).

Given the predicted role of HYAL2 in initiating the degradation of HA by cleavage of high molecular mass HA to smaller fragments for internalization, we expected that the HA found in the tissues of *Hyal2* KO mice would have a larger molecular mass than that in control animals. To assess this, HA was partially purified from the sera and hearts of *Hyal2* KO and control mice, and its size was analyzed by agarose gel electrophoresis. Accumulating HA was clearly evident in the hearts (Fig. 9*D*) and sera (Fig. 9*E*) of *Hyal2* KO mice compared with control mice. The size of the HA in *Hyal2* KO mice was also increased compared with that in control tissues (Fig. 9, *D* and *E*). The size of the isolated HA did not differ between acute and non-acute *Hyal2* KO mice (data not shown). The material that we identified as HA in Fig. 9 (*D* and *E*) was readily digested with hyaluronidase SD, as shown in Fig. 9*F*, verifying its identity. Some of the lower molecular mass bands did not digest with HYAL and are presumably other GAGs or contaminating proteins.

DISCUSSION

In this study, we have demonstrated that HYAL2 is essential for cardiopulmonary function in mice. In its absence, extracellular HA accumulates in the serum and the interstitium of the heart muscle and lungs, heart valves thicken, and pulmonary fibrosis develops in some animals, leading to severe cardiopulmonary dysfunction and premature death. This cardiopulmonary failure follows an acute course (mean survival of ~3 months) in some animals and a subacute course (mean survival of <6 months) in others. Acutely affected animals exhibited severe atrial dilation, cardiac hypertrophy, and pulmonary fibrosis, which were absent in subacute animals. However, increasing plasma HA levels, heart valvulopathy, myocardial infiltration with GAGs and HA, and influx of pulmonary macrophages were present in all *Hyal2* KO mice, confirming a major role of HYAL2 in cardiopulmonary function and possibly in overall HA turnover. Indeed, using HABP, we found increased HA levels in most tissues of both acute and non-acute *Hyal2* KO mice.[4] Previous examinations of *Hyal2* KO mice had revealed preweaning lethality, bone abnormalities, mild anemia, and elevated serum HA (16).

Whether or not *Hyal2* KO mice develop the more severe acute phenotype is likely determined by other genetic loci. Indeed, the heart phenotype is infrequent on the C57BL/6 background, and the frequency of preweaning lethality is lower on the C57BL/6 background (<10%) than on the outbred background (16%). Taken together, these findings suggest that other loci can strongly influence the phenotype associated with HYAL2 deficiency.

The heart may be especially susceptible to the effects of HYAL2 deficiency because of the high levels of HA in the developing heart (3). In contrast to HA synthase 2 KO mice, in which a deficiency of HA synthesis prevents the formation of the endocardial cushion and epithelial-to-mesenchymal transition (23, 24), the heart and valves appear to develop normally in *Hyal2* KO mice. However, an apparent failure to remove excess HA in the myocardium and valves after their formation, together with a possible ongoing failure of normal HA degradation, leads to postnatal cardiopulmonary dysfunction.

Heart valvular pathology of the *Hyal2* KO mice was not limited to the pulmonary valve, indicating that HYAL2 is important in the homeostasis of the valvular ECM in general. This is not surprising given that HA is a major GAG in heart valves and has viscoelastic properties that allow it to absorb shear force during the cardiac cycle (25). The valvular ECM is expanded and disorganized in various MPSs that result from mutations in GAG-degrading enzymes (14, 26). In addition, similar phenotypes result from defects in some ECM-remodeling enzymes, including a deficiency in the ADAMTS9 (a disintegrin and metalloproteinase with thrombospondin motifs 9) enzyme (27). Abnormalities in HA levels in valves have also been associated with common disorders such as myxomatous valve disease (28–30). Given the important role that HYAL2 can play in regulating HA levels, alterations in its level should be considered as a factor that could contribute to valve disease in humans. A complete deficiency of HYAL2 results in a severe phenotype, and therefore, it is less likely that a complete deficiency of HYAL2 is compatible with human life.

Mice with HYAL2 deficiency also had excess ECM and accumulating HA in the atrial myocardium. In the acute *Hyal2* KO mice, there were clearly increased levels of HA, although when the level of HA in the total heart was determined, no significant difference between acute and non-acute *Hyal2* KO mice was detected. It is possible that as the heart attempts to respond to the stress placed on it by abnormal valve function, additional ECM is synthesized, and HA then accumulates. Interestingly, we did not find HA accumulation in the ventricular myocardium, suggesting that *Hyal2* deficiency impacts the atrial more than the ventricular myocardium.

HA can make fluids highly viscous, and higher plasma viscosity can increase circulatory resistance and induce or aggravate heart failure (31), possibly leading to cardiac hypertrophy and pulmonary edema. This, in turn, could result in the accumulation of α-SMA and collagen, which is seen in acutely affected *Hyal2* KO mice. However, we have no pathological evidence for such a chain of events. Although the contribution of elevated serum HA to the phenotype of *Hyal2* KO mice is unclear, it is interesting to compare it with the phenotype resulting from a deficiency of a major receptor of HA, HARE (hyaluronan receptor for endocytosis) (32). Interestingly, *Hare* KO mice have been reported to show high levels of serum HA, dilated cardiomyopathy, and premature mortality (33). These findings provide further evidence that a disturbance in extracellular HA is responsible for the cardiac phenotype seen in *Hyal2* KO mice.

An alternative explanation for the observed lung pathology in acute mice is that a failure to degrade HA results in a primary defect in lung development (34). The smaller size, cardiomyocyte pathology, and atrial dilation in acute *Hyal2* KO mice could be secondary to impaired lung function. The numerous alveolar and interstitial macrophages in the lungs of *Hyal2* KO mice may indicate the attempt to reduce the interstitial deposits of HA and collagen. Such developmental delay could also cause high preweaning lethality in *Hyal2* KO mice.

[4] B. Chowdhury, R. Hemming, and B. Triggs-Raine, unpublished data.

HYAL2 is one of six hyaluronidase genes in humans and seven in mice (35). It is a glycosylphosphatidylinositol-anchored protein with a neutral pH optimum and a preference to cleave high molecular mass HA into 20-kDa fragments (1). Most studies indicate that HYAL2 functions at the cell surface and has therefore been proposed to degrade extracellular HA to smaller fragments that are internalized for further degradation (36). Our findings support this model, as the level of serum HA was extremely high, whereas the level of circulating HA has not been shown to be elevated in mouse models with HYAL1 or HYAL3 deficiency. The larger size of the HA that we detected in *Hyal2* KO tissues and serum also supports a role for HYAL2 in cleaving HA to smaller fragments for internalization. Furthermore, electron microscopy indicates that the accumulating material in the *Hyal2* KO mice is extracellular, whereas the material appears to be intracellular in humans that are deficient in HYAL1 (9). The phenotype observed in *Hyal2* KO mice is much more severe than that in *Hyal1*- and *Hyal3*-deficient mice (15, 17) and more similar to that seen in other forms of MPS. This may be due to a redundancy in the intracellular pathway of HA degradation, but no other enzyme can substitute for HYAL2 in extracellular degradation.

Finally, in 43% of the surviving *Hyal2* KO mice, we found that one kidney was missing. Interestingly, the kidney is another organ that has high levels of HA during development (37), so like the heart, it may be more susceptible to defects due to HA accumulation. In the longer term, studies of *Hyal2* KO mice at different embryonic and preweaning stages will help to identify those tissues where HA degradation by HYAL2 is critical.

In conclusion, this study illustrates the importance of HYAL2 in HA degradation in the heart and in normal cardiopulmonary function. Localized extracellular accumulation of HA in the KO mice results in a storage disorder that is different from classic MPS disorders, where the storage is typically both lysosomal and extracellular. Although a human condition resulting from alterations in HYAL2 activity has not yet been described, it will be interesting to examine the levels of HYAL2 and the serum HA concentration in patients with unexplained heart valve abnormalities.

REFERENCES

1. Lepperdinger, G., Müllegger, J., and Kreil, G. (2001) Hyal2–less active, but more versatile? *Matrix Biol.* **20,** 509–514
2. Andre, B., Duterme, C., Van Moer, K., Mertens-Strijthagen, J., Jadot, M., and Flamion, B. (2011) Hyal2 is a glycosylphosphatidylinositol-anchored, lipid raft-associated hyaluronidase. *Biochem. Biophys. Res. Commun.* **411,** 175–179
3. Camenisch, T. D., Spicer, A. P., Brehm-Gibson, T., Biesterfeldt, J., Augustine, M. L., Calabro, A., Jr., Kubalak, S., Klewer, S. E., and McDonald, J. A. (2000) Disruption of hyaluronan synthase-2 abrogates normal cardiac morphogenesis and hyaluronan-mediated transformation of epithelium to mesenchyme. *J. Clin. Invest.* **106,** 349–360
4. Csóka, A. B., Scherer, S. W., and Stern, R. (1999) Expression analysis of six paralogous human hyaluronidase genes clustered on chromosomes 3p21 and 7q31. *Genomics* **60,** 356–361
5. Hascall, V., Sandy, J. D., and Handley, C. J. (1999) in *Biology of the Synovial Joint* (Caterson, B., Archer, C. W., Benjamin, M., and Ralphs, J., eds) pp. 101–120, Harwood Academic Publishers, The Netherlands
6. Stern, R. (2003) Devising a pathway for hyaluronan catabolism: are we there yet? *Glycobiology* **13,** 105R–115R
7. Bourguignon, L. Y., Singleton, P. A., Diedrich, F., Stern, R., and Gilad, E. (2004) CD44 interaction with Na^+-H^+ exchanger (NHE1) creates acidic microenvironments leading to hyaluronidase-2 and cathepsin B activation and breast tumor cell invasion. *J. Biol. Chem.* **279,** 26991–27007
8. Chow, G., Knudson, C. B., and Knudson, W. (2006) Expression and cellular localization of human hyaluronidase-2 in articular chondrocytes and cultured cell lines. *Osteoarthritis Cartilage* **14,** 849–858
9. Natowicz, M. R., Short, M. P., Wang, Y., Dickersin, G. R., Gebhardt, M. C., Rosenthal, D. I., Sims, K. B., and Rosenberg, A. E. (1996) Clinical and biochemical manifestations of hyaluronidase deficiency. *N. Engl. J. Med.* **335,** 1029–1033
10. Triggs-Raine, B., Salo, T. J., Zhang, H., Wicklow, B. A., and Natowicz, M. R. (1999) Mutations in *HYAL1*, a member of a tandemly distributed multigene family encoding disparate hyaluronidase activities, cause a newly described lysosomal disorder, mucopolysaccharidosis IX. *Proc. Natl. Acad. Sci. U.S.A.* **96,** 6296–6300
11. Armstrong, E. J., and Bischoff, J. (2004) Heart valve development: endothelial cell signaling and differentiation. *Circ. Res.* **95,** 459–470
12. Hinton, R. B., and Yutzey, K. E. (2011) Heart valve structure and function in development and disease. *Annu. Rev. Physiol* **73,** 29–46
13. Braunlin, E. A., Harmatz, P. R., Scarpa, M., Furlanetto, B., Kampmann, C., Loehr, J. P., Ponder, K. P., Roberts, W. C., Rosenfeld, H. M., and Giugliani, R. (2011) Cardiac disease in patients with mucopolysaccharidosis: presentation, diagnosis and management. *J. Inherit. Metab. Dis.* **34,** 1183–1197
14. Jordan, M. C., Zheng, Y., Ryazantsev, S., Rozengurt, N., Roos, K. P., and Neufeld, E. F. (2005) Cardiac manifestations in the mouse model of mucopolysaccharidosis I. *Mol. Genet. Metab.* **86,** 233–243
15. Atmuri, V., Martin, D. C., Hemming, R., Gutsol, A., Byers, S., Sahebjam, S., Thliveris, J. A., Mort, J. S., Carmona, E., Anderson, J. E., Dakshinamurti, S., and Triggs-Raine, B. (2008) Hyaluronidase 3 (*HYAL3*) knockout mice do not display evidence of hyaluronan accumulation. *Matrix Biol.* **27,** 653–660
16. Jadin, L., Wu, X., Ding, H., Frost, G. I., Onclinx, C., Triggs-Raine, B., and Flamion, B. (2008) Skeletal and hematological anomalies in HYAL2-deficient mice: a second type of mucopolysaccharidosis IX? *FASEB J.* **22,** 4316–4326
17. Martin, D. C., Atmuri, V., Hemming, R. J., Farley, J., Mort, J. S., Byers, S., Hombach-Klonisch, S., Csoka, A. B., Stern, R., and Triggs-Raine, B. L. (2008) A mouse model of human mucopolysaccharidosis IX exhibits osteoarthritis. *Hum. Mol. Genet.* **17,** 1904–1915
18. Allen, T. C. (1994) in *Laboratory Methods in Histotechnology*, (Prophet, E. B., Mills, B., Arrington, J. B., and Sobin, L. H., eds) pp. 53–58, American Registry of Pathology, Washington, D.C.
19. Gaffney, E. (1994) in *Laboratory Methods in Histotechnology*, (Prophet, E. B., Mills, B., Arrington, J. B., and Sobin, L. H., eds) pp. 149–174, American Registry of Pathology, Washington, D.C.
20. Gushulak, L., Hemming, R., Martin, D., Seyrantepe, V., Pshezhetsky, A., and Triggs-Raine, B. (2012) Hyaluronidase 1 and β-hexosaminidase have redundant functions in hyaluronan and chondroitin sulfate degradation. *J. Biol. Chem.* **287,** 16689–16697
21. Plaas, A. H., West, L., Midura, R. J., and Hascall, V. C. (2001) Disaccharide composition of hyaluronan and chondroitin/dermatan sulfate. Analysis with fluorophore-assisted carbohydrate electrophoresis. *Methods Mol. Biol.* **171,** 117–128
22. Gordon, L. B., Harten, I. A., Calabro, A., Sugumaran, G., Csoka, A. B., Brown, W. T., Hascall, V., and Toole, B. P. (2003) Hyaluronan is not elevated in urine or serum in Hutchinson-Gilford progeria syndrome. *Hum. Genet.* **113,** 178–187
23. Camenisch, T. D., Biesterfeldt, J., Brehm-Gibson, T., Bradley, J., and McDonald, J. A. (2001) Regulation of cardiac cushion development by hyaluronan. *Exp. Clin. Cardiol.* **6,** 4–10
24. Camenisch, T. D., Schroeder, J. A., Bradley, J., Klewer, S. E., and McDonald, J. A. (2002) Heart-valve mesenchyme formation is dependent on hyaluronan-augmented activation of ErbB2-ErbB3 receptors. *Nat. Med.* **8,** 850–855
25. Stephens, E. H., Chu, C. K., and Grande-Allen, K. J. (2008) Valve proteoglycan content and glycosaminoglycan fine structure are unique to microstructure, mechanical load and age: relevance to an age-specific tissue-engineered heart valve. *Acta Biomater.* **4,** 1148–1160

26. Strauch, O. F., Stypmann, J., Reinheckel, T., Martinez, E., Haverkamp, W., and Peters, C. (2003) Cardiac and ocular pathologies in a mouse model of mucopolysaccharidosis type VI. *Pediatr. Res.* **54,** 701–708
27. Kern, C. B., Wessels, A., McGarity, J., Dixon, L. J., Alston, E., Argraves, W. S., Geeting, D., Nelson, C. M., Menick, D. R., and Apte, S. S. (2010) Reduced versican cleavage due to *Adamts9* haploinsufficiency is associated with cardiac and aortic anomalies. *Matrix Biol.* **29,** 304–316
28. Stephens, E. H., Saltarrelli, J. G., Baggett, L. S., Nandi, I., Kuo, J. J., Davis, A. R., Olmsted-Davis, E. A., Reardon, M. J., Morrisett, J. D., and Grande-Allen, K. J. (2011) Differential proteoglycan and hyaluronan distribution in calcified aortic valves. *Cardiovasc. Pathol.* **20,** 334–342
29. Gupta, V., Barzilla, J. E., Mendez, J. S., Stephens, E. H., Lee, E. L., Collard, C. D., Laucirica, R., Weigel, P. H., and Grande-Allen, K. J. (2009) Abundance and location of proteoglycans and hyaluronan within normal and myxomatous mitral valves. *Cardiovasc. Pathol.* **18,** 191–197
30. Vyavahare, N., Ogle, M., Schoen, F. J., Zand, R., Gloeckner, D. C., Sacks, M., and Levy, R. J. (1999) Mechanisms of bioprosthetic heart valve failure: fatigue causes collagen denaturation and glycosaminoglycan loss. *J. Biomed. Mater. Res.* **46,** 44–50
31. Hoffmeister, A., Hetzel, J., Sander, S., Kron, M., Hombach, V., and Koenig, W. (1999) Plasma viscosity and fibrinogen in relation to haemodynamic findings in chronic congestive heart failure. *Eur. J. Heart Fail.* **1,** 293–295
32. Falkowski, M., Schledzewski, K., Hansen, B., and Goerdt, S. (2003) Expression of stabilin-2, a novel fasciclin-like hyaluronan receptor protein, in murine sinusoidal endothelia, avascular tissues, and at solid/liquid interfaces. *Histochem. Cell Biol.* **120,** 361–369
33. Schledzewski, K., Géraud, C., Arnold, B., Wang, S., Gröne, H. J., Kempf, T., Wollert, K. C., Straub, B. K., Schirmacher, P., Demory, A., Schönhaber, H., Gratchev, A., Dietz, L., Thierse, H. J., Kzhyshkowska, J., and Goerdt, S. (2011) Deficiency of liver sinusoidal scavenger receptors stabilin-1 and -2 in mice causes glomerulofibrotic nephropathy via impaired hepatic clearance of noxious blood factors. *J. Clin. Invest.* **121,** 703–714
34. Underhill, C. B., Nguyen, H. A., Shizari, M., and Culty, M. (1993) CD44 positive macrophages take up hyaluronan during lung development. *Dev. Biol.* **155,** 324–336
35. Csóka, A. B., Frost, G. I., Heng, H. H., Scherer, S. W., Mohapatra, G., Stern, R., and Csóka, T. B. (1998) The hyaluronidase gene *HYAL1* maps to chromosome 3p21.2-p21.3 in human and 9F1-F2 in mouse, a conserved candidate tumor suppressor locus. *Genomics* **48,** 63–70
36. Stern, R. (2004) Hyaluronan catabolism: a new metabolic pathway. *Eur. J. Cell Biol.* **83,** 317–325
37. Pohl, M., Sakurai, H., Stuart, R. O., and Nigam, S. K. (2000) Role of hyaluronan and CD44 in *in vitro* branching morphogenesis of ureteric bud cells. *Dev. Biol.* **224,** 312–325